J. Fluid Mech. (1981), *vol.* 103, *pp.* 321–344
Printed in Great Britain

An experimental study of critical layers

By S. A. THORPE

Institute of Oceanographic Sciences,
Wormley, Godalming, Surrey

(Received 20 February 1980 and in revised form 22 June 1980)

Laboratory experiments have been made to investigate the development of internal gravity waves as they approach a critical layer where their phase speed is equal to that of the mean flow. The waves are produced in the accelerating flow of a stratified fluid in a long tilted tube in which the lower boundary has sinusoidal corrugations. As found in earlier experiments, the waves are not observed to propagate beyond the critical layer. Near the layer their amplitude increases, with the development of regions in which the fluid is gravitationally unstable. Kelvin–Helmholtz instability is not observed, perhaps because of viscous effects.

A model is devised which describes the weakly nonlinear development of the waves. This is solved numerically. The results compare favourably with the experiments until gravitational instability is imminent. The numerical model is used to estimate both the second order Eulerian 'jet', which develops below the critical layer, and the Stokes drift. In the cases examined, the maximum drift is stronger than the jet and opposite in direction. The numerical model predicts the regions of wave breaking quite well.

Internal gravity waves in the ocean may be modified by transient critical layers, for example those caused by vertically-propagating near-inertial oscillations.

1. Introduction

The change in the structure of internal gravity waves as they approach a critical layer has been a topic of much interest since the effect of critical layers was demonstrated by Booker & Bretherton (1967). A critical level is one at which the horizontal phase velocity of approaching internal gravity waves is equal to the speed of the mean flow, supposed horizontal, although, perhaps more significantly, it is a level at which the vertical group velocity of packets of infinitesimal waves tends to zero sufficiently rapidly that the waves are prevented from propagating further in a vertical direction (Bretherton 1966). Singularities of this kind are features common to waves travelling in variable media (for others, see Acheson 1976; Peregrine & Thomas 1979; Stewartson 1978; Grimshaw 1980).

Analytical and numerical studies, for example those of Hazel (1967), Jones (1968), Breeding (1971), Tanaka (1975), Geller, Tanaka & Fritts (1975), Fritts & Geller (1976), Fritts (1978, 1979); McIntyre & Weissman (1978) and Brown & Stewartson (1980*a*) have done much to clarify the linear, and some of the nonlinear, processes which affect internal gravity waves near critical layers. Linear theory has been found to describe the interaction between the waves and the mean flow if the Richardson number exceeds two (Breeding 1971). The importance of critical layer absorption as a process

0022-1120/81/4660-2970 $02.00

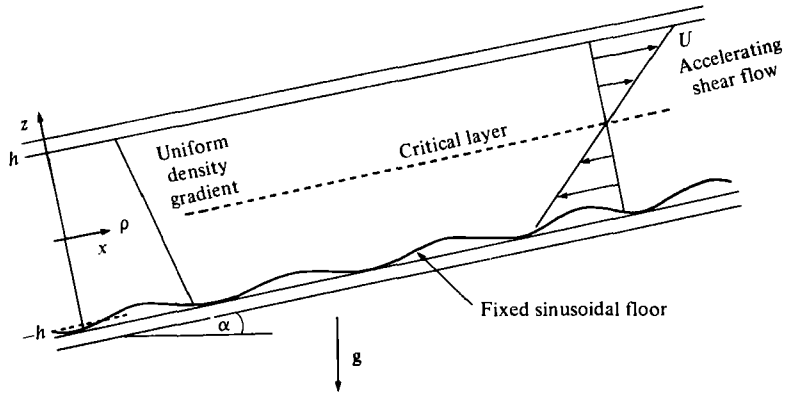

FIGURE 1. The apparatus; an inclined tube with a corrugated floor.

in the atmosphere was recognized from the first, and many observations of wave-like structures detected by radar or acoustic soundings have been ascribed to the effects of critical layers (see for example Merrill 1977; Eymard & Weill 1979; Klostermeyer 1980). There is however, some confusion in the literature about the distinction between waves at critical layers and the transient waves which develop during shear flow (or Kelvin–Helmholtz) instability, and in interpreting observations the features which distinguish one from another may be difficult to detect. Munk (1980) has recently advocated an assessment of the role of critical layers in relation to the development of the spectrum of internal gravity waves in the ocean.

The precise nature of the flow in the vicinity of a critical layer is however not altogether clear, and we know of only two, somewhat cursory, laboratory investigations of the phenomenon which have been made (appendix by Bretherton *et al.* to the paper by Hazel 1967; Thorpe 1973*a*). Both these experiments fall in a range in which Fritts & Geller (1976) find that viscous effects are likely to promote the stability of the waves at the critical level.

We have made some further experiments in a tilting tube. The tube is filled with a stratified brine solution and flow is generated by tilting the tube away from a horizontal position. In the earlier experiments, waves were generated in the lee of a small triangular obstacle attached to the floor of the tube. In the present experiments the floor has a sinusoidal corrugation (see figure 1), and the internal waves which develop have a well defined wavelength and are more amenable to theoretical description.

In § 2 we describe the experiments and the development of the waves and in § 3 we discuss, and compare with experiments, a numerical model which includes weakly non-linear effects. The value of this comparison is that quantities which may be calculated accurately in the model but which are very difficult to measure in the experiments (for example, the velocity distribution), can be estimated with some confidence provided, of course, that there is agreement between the quantities which *can* be measured in the experiment (in particular, the wave amplitude and phase) and those which are predicted by the model.

As a preliminary we consider the propagation of a packet of internal gravity waves in fluid of Brunt–Väisälä frequency, N, in a horizontal shear flow, $U(z,t)$, z being vertically upwards. We suppose that the W.K.B. approximation is valid so that the

group velocity is determined locally. We shall consider the paths of internal gravity waves formed as stationary lee waves in an accelerating flow over the sinusoidal flow of the tube.

Following Bretherton (1966), the frequency of a two-dimensional internal gravity wave of wavenumber (k, m) relative to a fixed frame of reference is

$$\sigma = kU - \omega, \tag{1}$$

where ω is the frequency measured in a frame of reference moving with the local flow;

$$\omega^2 = \frac{N^2k^2}{k^2+m^2}.$$

Following Garrett (1967, equation (1.8))

$$d\sigma/dt = k\,\partial U/\partial t, \tag{2}$$

where $d/dt \equiv \partial/\partial t + \mathbf{c}_g \cdot \nabla$ is the derivative following a wave packet moving at speed $\mathbf{c}_g$.

From (1) and (2) and assuming uniformity in the x direction we find

$$d\omega/dt = -kc_{gv}\,\partial U/\partial z \tag{3}$$

where $c_{gv} = \partial\omega/\partial m = \omega^2(N^2-\omega^2)^{\frac{1}{2}}/N^2k$ is the vertical group velocity. We take k to be the wavenumber of the corrugations in the flow of the tube. In the laboratory experiments described in § 2, N is constant, and we take

$$U(z,t) = N^2zt\sin\alpha, \tag{4}$$

corresponding to the flow in the absence of corrugations (Thorpe 1968*a*), where t is the time elapsed after the tube is tilted through an angle α. Hence (3) gives

$$\frac{d\omega}{dt} = -\omega^2(N^2-\omega^2)^{\frac{1}{2}}t\sin\alpha,$$

which has a solution independent of

$$\begin{aligned}\frac{(N^2-\omega^2)^{\frac{1}{2}}}{\omega} &= \frac{(\tau^2-\tau_0^2)}{2}\sin\alpha + \frac{(1-k^2h^2\tau_0^2\sin^2\alpha)^{\frac{1}{2}}}{kh\tau_0\sin\alpha}\\ &= \frac{\tau^2}{2}\sin\alpha + q, \quad \text{say,}\end{aligned} \tag{5}$$

where $\tau = Nt$, $\tau_0 = Nt_0$ and t_0 is the time at which the wave packet originates with frequency $\sigma = 0$ at $z = -h$, the floor of the tube. Using this solution for ω we can now find the height z of the wave packet by integrating

$$dz/dt = c_{gv},$$

to give, using (5)

$$Z = \int_{\tau_0}^{\tau} \frac{(q+\frac{1}{2}\tau^2\sin\alpha)\,d\tau}{[1+(q+\frac{1}{2}\tau^2\sin\alpha)^2]^{\frac{1}{2}}} - kh,$$

where $Z = kz$, and $z = -h$ when $t = t_0$. Integration was made numerically using a Runge–Kutta technique with values of $kh = 1$ and 2 and $\sin\alpha = 0{\cdot}1$ which correspond approximately to the parameters used in the experiments. Figure 2 shows the wave paths in the (τ, Z) plane. The height of the wave front, a caustic surface, increases

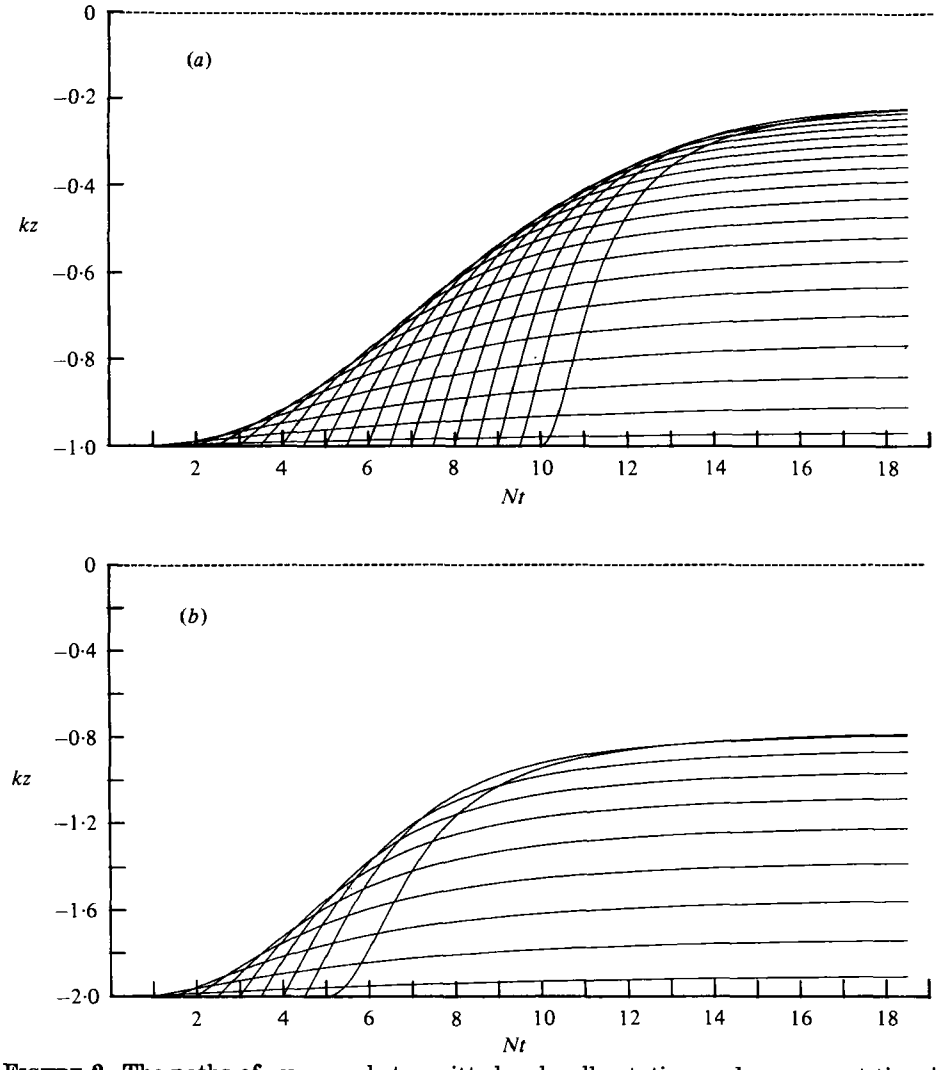

FIGURE 2. The paths of wave packets emitted as locally stationary lee waves at time intervals $0{\cdot}5N^{-1}$ from the level of the bottom of the tube for (*a*) $kh = 1{\cdot}0$ and (*b*) $kh = 2{\cdot}0$, with $\sin\alpha = 0{\cdot}1$.

with time, waves emitted at later times overtaking their predecessors. Even at $\tau = 18$ the waves are some way from the level $z = 0$ where the mean flow vanishes. The vertical wavenumber of stationary waves at the flow is

$$m = k\left(\frac{1}{\tau^2 k^2 h^2 \sin^2\alpha} - 1\right)^{\frac{1}{2}}, \tag{6}$$

whilst there

$$c_{gv} = \frac{k^2 U^3(-h,t)}{N^2}\left(\frac{1}{\tau^2 k^2 h^2 \sin^2\alpha} - 1\right)^{\frac{1}{2}} \tag{7}$$

and so for $\tau > (kh\sin\alpha)^{-1}$, m and c_{gv} become imaginary and waves can no longer radiate from the floor. The rays therefore appear at $Z = -kh$ only in $0 < \tau < (kh\sin\alpha)^{-1}$.

The Richardson number of the flow is $R_i = (\tau\sin\alpha)^{-1}$ and this eventually becomes

small. Figure 2 is strictly valid only for infinitesimal waves of scales much less than those of the mean flow and for large mean flow Richardson numbers (Bretherton 1966) and may therefore serve only as a rough guide for the experiments.

In regard to the confusion between critical layer absorption and critical layer instability, it is pertinent to note that the steady flow of a fluid with constant shear and constant Brunt–Väisälä frequency appears to be stable to infinitesimal disturbances for all positive values of the Richardson number (Brown & Stewartson 1980*b*). A similar flow which is uniformly accelerating appears also to be stable (Thorpe 1978*a*).

2. The experiments

The apparatus was a 4·85 m long, 10 cm wide, 16 cm high rectangular tube with perspex side walls, which could be rotated about a central horizontal axis normal to its length (figure 1). A false floor was placed in the bottom of the tube carrying an approximately sinusoidal wave form (it can be seen in figures 3 etc.) made of flexible aluminium sheet supported by blocks and screwed to a rigid base plate. The volume between the sheet and the plate was filled with wax or plasticene. Three different corrugated floors were used; two had 16 undulations of 25 cm wavelength and wave heights of 0·5 and 1·0 cm, which reduced the mean tube depth to 14·85 and 14·7 cm respectively, and a third had 8 undulations of 50 cm wavelength and 1·0 cm height which reduced the mean tube depth to 14·7 cm. To aid the removal of air bubbles and to reduce the effects of mixing during filling, the tube was filled in a tilted position (at about 25 deg to the horizontal) with brine solution to the required density profile, normally a constant gradient. Potassium permanganate dye was added during filling to mark surfaces of constant density. Once full, the tube was slowly rotated into a horizontal position and left until the fluid had settled. A little mixing occurred as the density surfaces spread over the corrugated bottom but, with care, this was small. Some exchange was possible between the troughs of neighbouring undulations through small gaps left between the false floor and the side walls. It was sometimes difficult to exclude all air from the tube, and in several cases a few bubbles trapped beneath the false floor were released during the experiment and can be seen in some of the photographs (e.g. figure 3) moving along the top boundary of the tube. These were, however, small and did not appear to affect the waves to any appreciable extent.

The experimental conditions were not ideal, for the surfaces of constant density were initially horizontal and pools of relatively dense fluid lay in the troughs of the corrugated bottom. It was impossible to fill the troughs with a specified density gradient. Moreover, because there was no salt flux through the bottom, the density gradient at this boundary was zero. The constant density gradient, assumed in the analysis of § 3, was thus not closely maintained below the level of the crests of the waves in the corrugated boundary.

The experiment consisted of sharply tilting the tube through a small angle, initiating a shear flow (Thorpe 1968*a*). The development of waves generated by the flow over the topography was recorded by a 35 mm camera taking about 3 frames per second and a 16 mm ciné camera at 30 frames per second. The times of tilt and of the 35 mm camera frames were recorded by electrical pulses on an ultra-violet recorder.

Figures 3 and 4 show photographs of the waves in experiments with constant density gradients in which the tube tilt was maintained (figure 3) or in which the tube

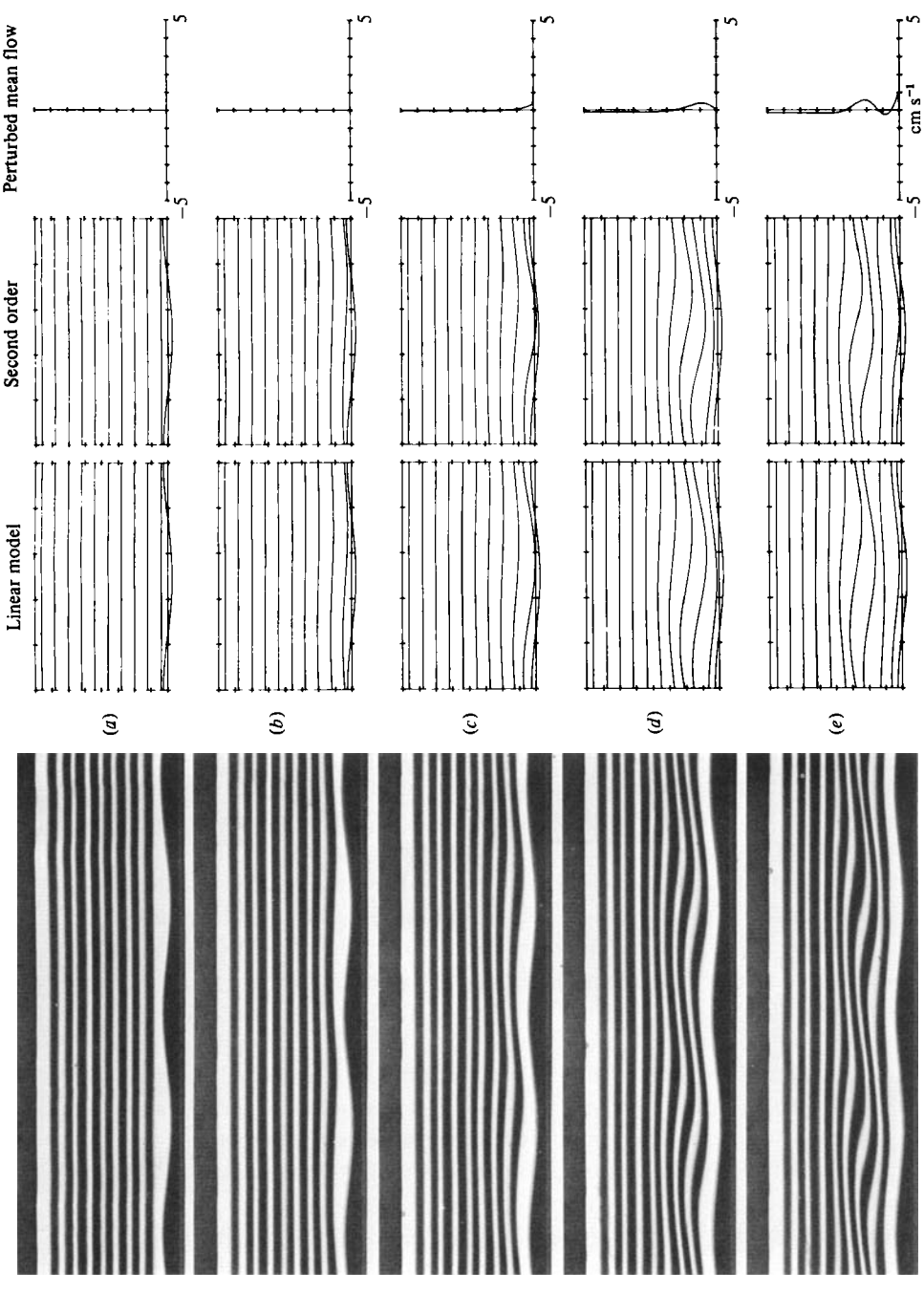

FIGURE 3. Waves in an accelerating shear flow over a corrugated floor of amplitude 0·5 cm and wavelength 25 cm. The tube contains stratified fluid with $N = 2{\cdot}626$ rad s^{-1} and has been tilted down to the left at $t = 0$ through 5·2 deg. Photographs of dye lines are shown at values of Nt (or mean flow Richardson number) of (*a*) 0(∞), (*b*) 2·91 (14·63), (*c*) 5·80 (3·68), (*d*) 8·72 (1·63), (*e*) 11·61 (0·92), (*f*) 14·52 (0·59), (*g*) 17·41 (0·41), (*h*) 20·32 (0·30), (*i*) 23·21 (0·23) and (*j*) 26·13 (0·18). At the right are shown plots of the density surfaces estimated using linear and second order models, and the mean second order Eulerian flow. The stippled areas are regions where the local Richardson number is less than 0·25, whilst the hatched areas are where the density gradient is negative.

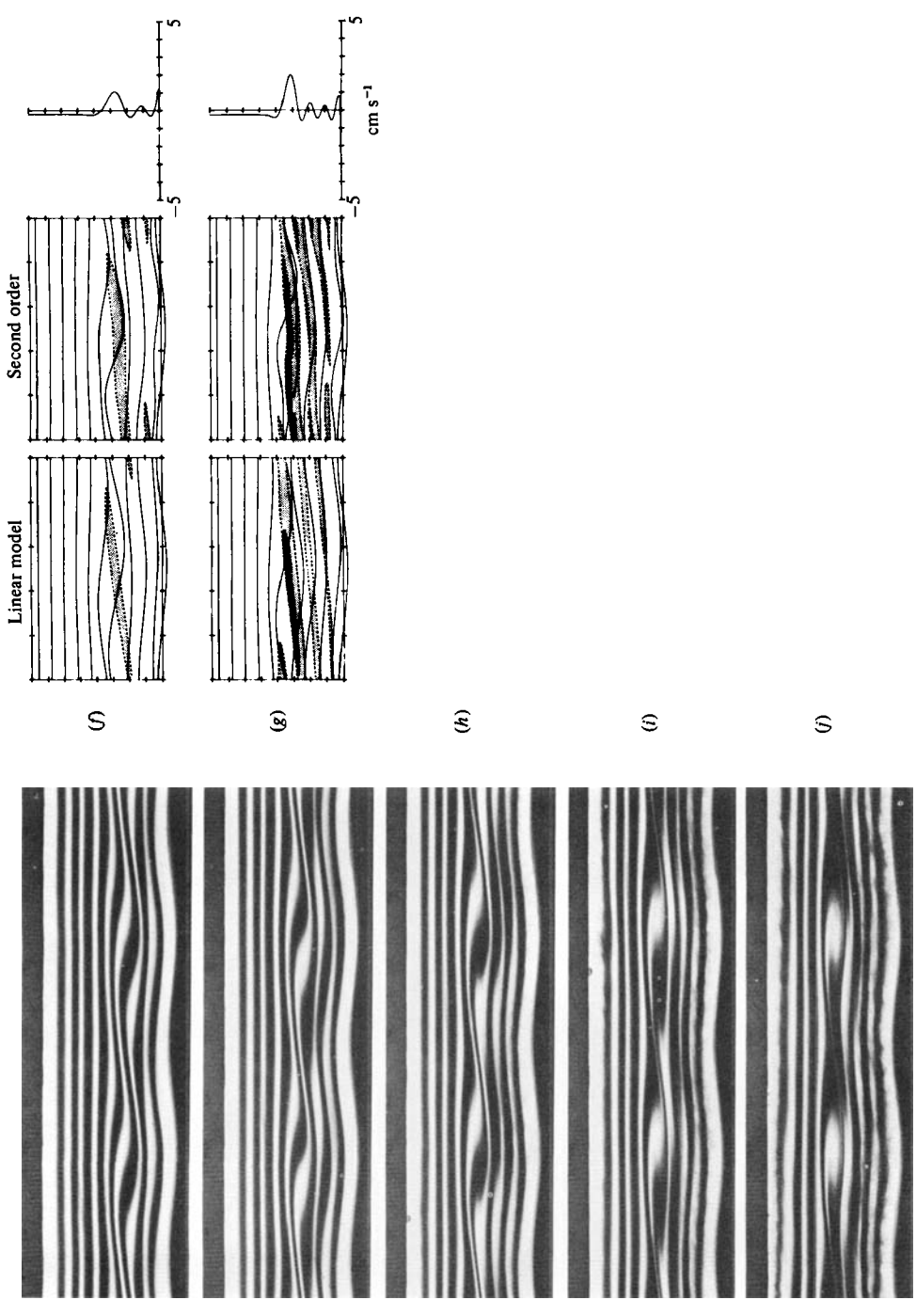

FIGURE 3. For legend see p. 326.

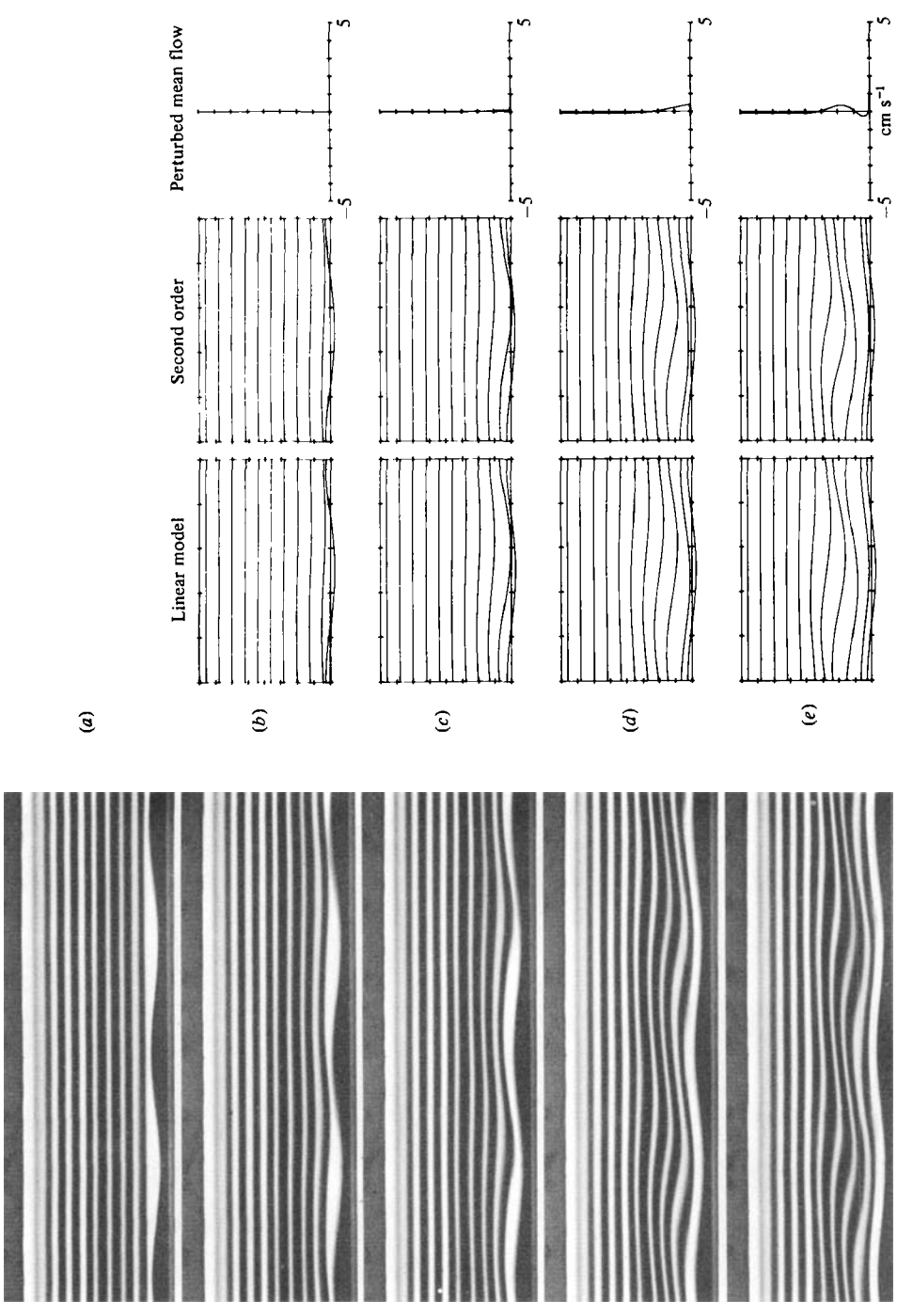

FIGURE 4. As for figure 3, but here $N = 2{\cdot}060$ rad s^{-1} and the tube has been tilted through 7·1 deg for 3·75 s ($Nt = 7{\cdot}72$) before being returned to the horizontal. The mean flow Richardson number was then 1·03. The photographs are at values of Nt of (*a*) 0, (*b*) 2·14, (*c*) 4·49, (*d*) 6·84, (*e*) 9·19, (*f*) 11·54, (*g*) 13·88, (*h*) 16·23, (*i*) 18·58 and (*j*) 20·93.

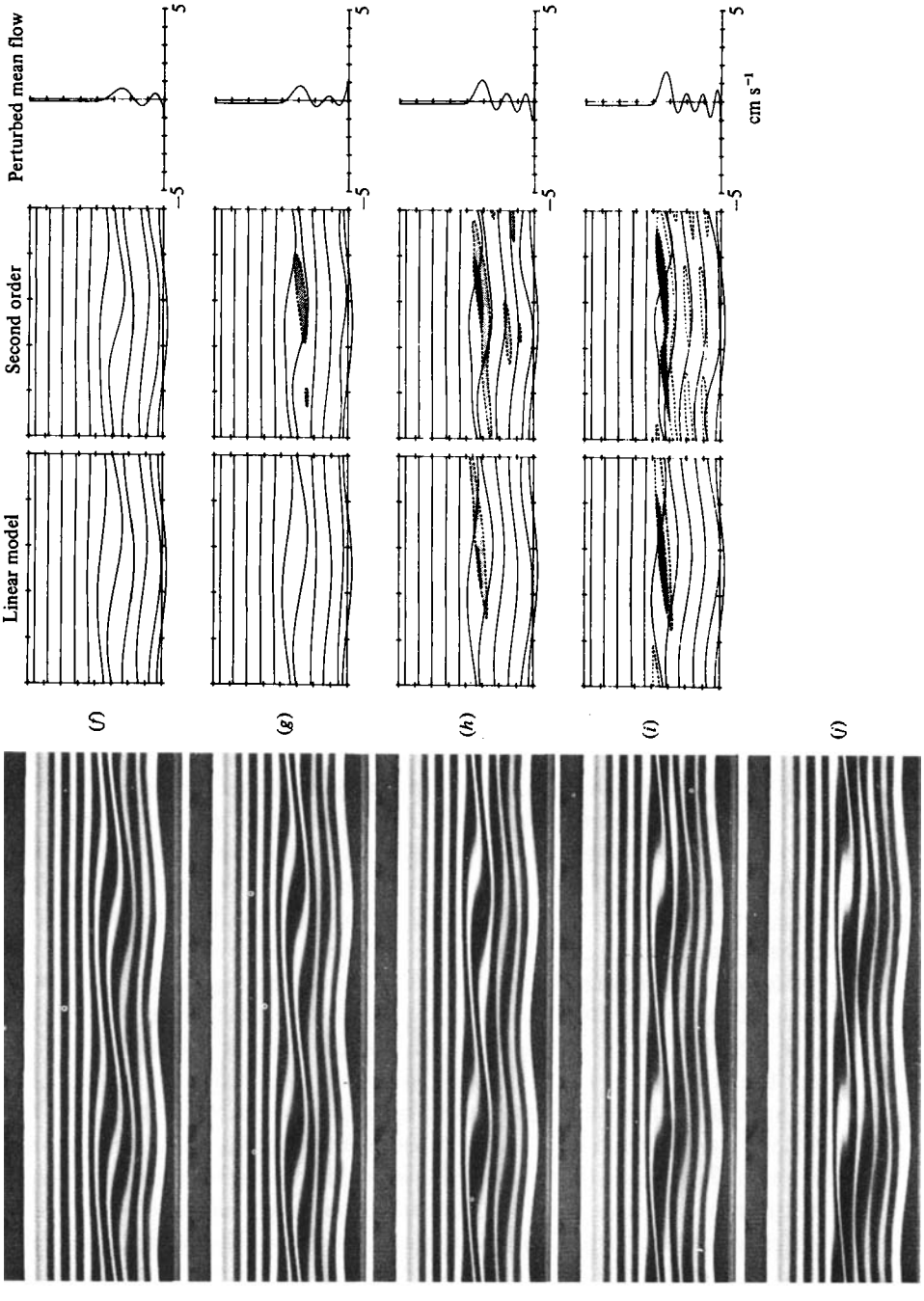

FIGURE 4. For legend see p. 328.

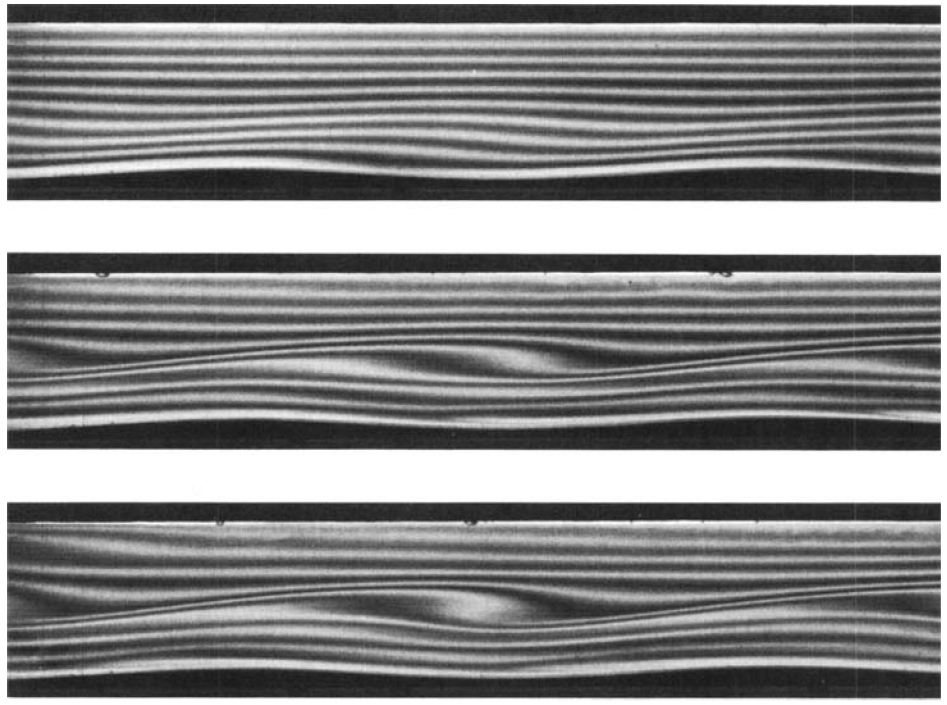

FIGURE 5. Waves in a flow above 0·5 cm amplitude corrugations of wavelength 50 cm. $N = 2{\cdot}487$ rad s^{-1} and $\alpha = 5{\cdot}3$ deg. The dyelines are shown at values of Nt (or mean Richardson number) of (*a*) 11·08 (0·96), (*b*) 21·63 (0·25), (*c*) 24·27 (0·20). In (*c*) the surge is entering at the left.

returned to the horizontal a few seconds after first being tilted (figure 4). In these and other photographs the tube was tilted down at the left and the flow near the floor of the tube is to the left, as shown in figure 1. Waves spread vertically away from the lower boundary with lines of constant phase tilting into the flow direction, that is towards the right. After a few seconds the slope of the dye lines to the right of the wave crests became steeper than that to the left, and the dye lines thickened where the slope was greatest and narrowed where it was least. The regions of reduced density gradient were subsequently advected through the wave pattern in the direction of the mean flow, whilst dye lines at higher levels, themselves now distorted by the waves, tended to thicken. This process of thickening, advection, and thickening at higher levels led to surfaces inclined at increasingly shallower angles to the horizontal, in which the density gradient was reduced and which subsequently appeared to be sites of gravitational overturn. The upward spread of the waves was arrested near mid-depth and there, or slightly below, the dye-line distortion occurred as an almost stationary process with gravitational overturn ensuing at a position almost immediately above the troughs of the corrugated floor. Between these sites of instability (and above the crests of the corrugations) the dye layers became very thin, and the overall pattern was similar to that found in Kelvin–Helmholtz instability at large amplitude (e.g. see Thorpe 1971, figure 12*d*). This wave development was found in both kinds of experiments although it occurred more rapidly when the flow continued to accelerate. The phase of the dye lines near the floor became approximately equal to that of the

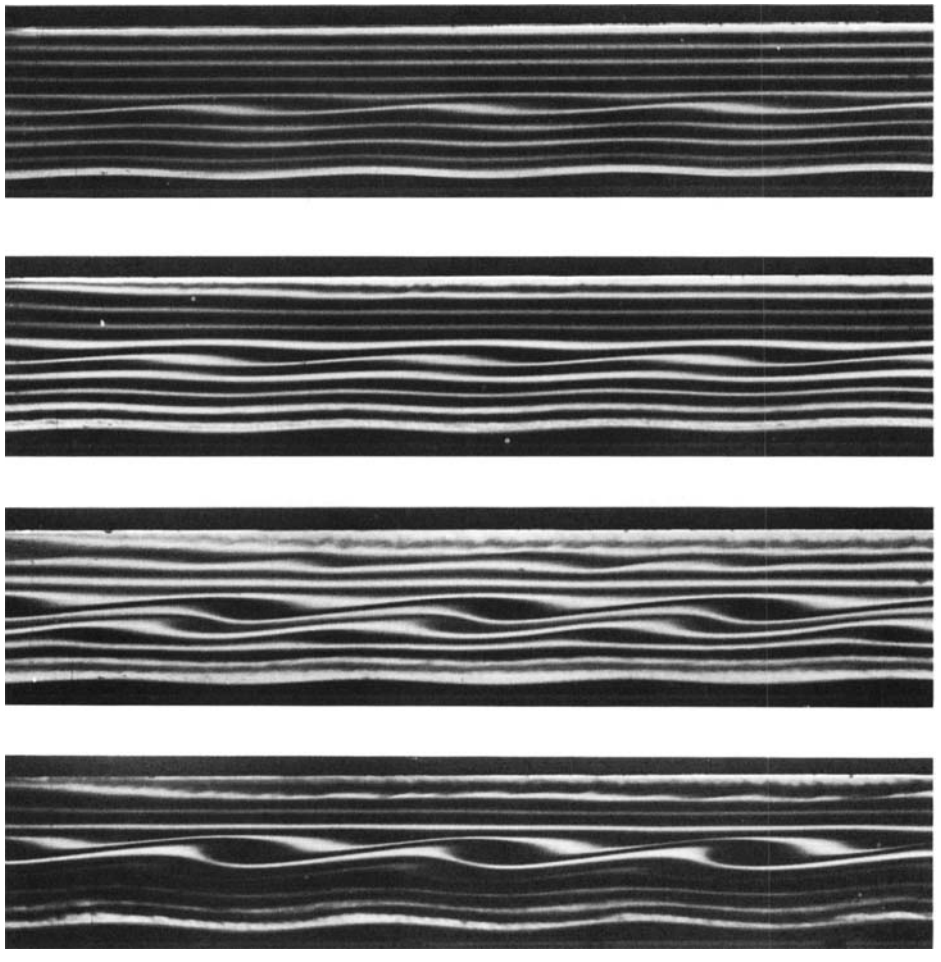

FIGURE 6. Waves above 0·25 cm amplitude corrugations of wavelength 25 cm. (*a*) $N = 2{\cdot}023$ rad s^{-1}, $\alpha = 7{\cdot}5$ deg, maintained for 3·98 s. Dyelines are shown at $Nt = 20{\cdot}67$ with mean flow Richardson number 0·88. (*b*) $N = 2{\cdot}601$ rad s^{-1}, $\alpha = 5{\cdot}1$ deg, tube remains tilted. Photo at $Nt = 22{\cdot}76$ at mean flow Richardson number 0·24. (*c*) $N = 2{\cdot}489$ rad s^{-1}, $\alpha = 10{\cdot}3$ deg, tube remained tilted. Photo at $Nt = 17{\cdot}00$ at mean flow Richardson number 0·11. (*d*) Waves above 0·5 cm amplitude corrugations of wavelength 25 cm. $N = 2{\cdot}674$ rads . s^{-1}, $\alpha = 10{\cdot}2$ deg, tube remained tilted. Photo at $N = 16, 15$ at mean flow Richardson number 0·12.

corrugations after a few seconds. Above the mid-depth level, the dye lines remained almost level, although slight undulations could be detected (e.g. figure 3*i*) at later times when the flow was allowed to continue acceleration. Small-scale disturbances advecting with the flow were seen in the final stages of the experiments. They were more prevalent near the lower boundary and possibly arose from an instability of the flow in the boundary layer where at this time the Reynolds number was large. The flow was eventually interrupted by the arrival of surges which propagated from the ends of the tube. Gravitational overturn is seen in figure 4 even though the mean flow Richardson number was greater than 0·25. Indeed it occurred in a region in which the second-order mean flow (see § 3) tended to reduce the shear.

Figure 5 shows the development of waves in an accelerating flow when the wavelength is 50 cm. The appearance of the waves is similar to that of figures 3 and 4, although the thickness of the unstable regions is increased. Figure 6 shows some other examples in accelerating flows, or flows in which the tube was returned to the horizontal, and at smaller mean flow Richardson numbers. The waves which can be seen near the upper boundary in figure 6(*d*) appeared to have originated locally although their wavelength was similar to that of the corrugations. Figure 6(*c*) shows simultaneous overturning at several levels.

3. Theory and numerical solutions

3.1. *The governing equations*

We consider the flow in the laboratory tube after it has been tilted at time $t = 0$ through an angle α. We neglect the effects of viscosity and diffusion, assume that the Boussinesq approximation is valid, that the flow is two dimensional, and that the tube is of great length, so that the effects of the surges can be neglected.

The equations of motion are:

$$\left(\frac{\partial}{\partial t}+U\frac{\partial}{\partial x}\right)\nabla^2\psi+J(\nabla^2\psi,\psi)=g\frac{\partial\rho}{\partial x}\cos\alpha-g\frac{\partial\rho}{\partial z}\sin\alpha \tag{8}$$

and

$$\left(\frac{\partial}{\partial t}+U\frac{\partial}{\partial x}\right)\rho+J(\rho,\psi)=-\frac{N^2}{g}\frac{\partial\psi}{\partial x}, \tag{9}$$

where the density is $\rho_0(0)\,(1-N^2z/g+\rho)$, $U = N^2tz\sin\alpha$, ψ is the stream function of the 'perturbed' flow and the axes x and z are taken as in figure 1. The perturbed flow is that caused by the presence of the corrugated floor and we shall suppose that it is small in comparison with U so that ψ and ρ may be expanded in terms of a small parameter ϵ

$$\psi=\epsilon\psi_1+\epsilon^2\psi_2+\ldots,\quad \rho=\epsilon\rho_1+\epsilon^2\rho_2+\ldots\,. \tag{10}$$

The boundary conditions are

$$\partial\psi/\partial x=0 \quad \text{at} \quad z=h, \tag{11}$$

and

$$\left(U+\frac{\partial\psi}{\partial z}\right)\frac{\partial\eta}{\partial x}=-\frac{\partial\psi}{\partial x} \quad \text{at} \quad z=-h+\eta(x), \tag{12}$$

where η is the equation of the corrugated floor,

$$\eta=a\epsilon\exp ikx,$$

where real parts are to be taken and a is a real constant.

Retaining only terms of order ϵ, we look for a solution for ψ, ρ periodic in x by introducing the non-dimensional variables ϕ, r where

$$\psi_1=\frac{N}{k^2}\phi(Z,\tau)\exp iX,\quad \rho_1=\frac{N^2}{gk}r(Z,\tau)\exp iX, \tag{13}$$

with $(X, Z) = (kx, kz)$ and $\tau = Nt$. Substituting in (8), (9), we find

$$\left(\frac{\partial}{\partial\tau}+iZ\tau\sin\alpha\right)\theta+\left(\sin\alpha\frac{\partial}{\partial Z}-i\cos\alpha\right)r=0, \tag{14}$$

and

$$\left(\frac{\partial}{\partial\tau}+iZ\tau\sin\alpha\right)r+i\phi=0, \tag{15}$$

where

$$\theta=\left(\frac{\partial^2}{\partial Z^2}-1\right)\phi. \tag{16}$$

These equations were derived elsewhere (Thorpe 1978*a*). The boundary and initial conditions however differ. The boundary conditions are now

$$\phi=0 \quad \text{at} \quad Z=kh$$

and

$$\phi=-AZ\tau\sin\alpha \quad \text{at} \quad Z=-kh,$$

where $A=ak$. (The latter condition implies that the net volume flux across a vertical section calculated to order ϵ is zero).

Numerical solutions of the equations (14), (15), with appropriate initial values, $\psi=\rho=0$, have been obtained following the method described by Thorpe (1978*a*). Using (15) to determine $r(Z,\tau+\Delta\tau)$ after a small time-step $\Delta\tau$ and then (14) to find $\theta(Z,\tau+\Delta\tau)$, (16) may be solved using a shooting method with the boundary conditions (17), (18) to give ϕ at $\tau+\Delta\tau$. Solutions were found for conditions corresponding to the laboratory experiments (see § 3.4). Whilst these provide an accurate description of the density field at small times, discrepancies are apparent at $\tau\sim 8$ when the Richardson number of the mean flow was about 1·5, and the density surfaces are no longer sinusoidal (see figure 3). To investigate the development of harmonics forced by non-linear terms we return to (8), (9), and retain terms of order ϵ^2, giving equations for ψ_2,ρ_2.

The governing equations can now be written

$$\left(\frac{\partial}{\partial\tau}+2iZ\tau\sin\alpha\right)\Theta+\left(\sin\alpha\frac{\partial}{\partial Z}-2i\cos\alpha\right)r_2=\frac{i}{2}\left(\phi\frac{\partial\theta}{\partial Z}-\theta\frac{\partial\phi}{\partial Z}\right), \tag{17}$$

$$\frac{\partial U_2}{\partial\tau}=\frac{i}{4}(\theta^*\phi-\theta\phi^*)+F(\tau), \tag{18}$$

$$\left(\frac{\partial}{\partial\tau}+2iZ\tau\sin\alpha\right)r_2+2i\phi_2=\frac{i}{2}\left(\phi\frac{\partial r}{\partial Z}-r\frac{\partial\phi}{\partial Z}\right), \tag{19}$$

and

$$\frac{\partial r_{20}}{\partial\tau}=\frac{i}{4}\frac{\partial}{\partial Z}(r^*\phi-r\phi^*), \tag{20}$$

where

$$\Theta=\left(\frac{\partial^2}{\partial Z^2}-4\right)\phi_2,$$

$$\psi_2=\frac{N}{k^2}[\phi_2(Z,\tau)\exp 2iX+\phi_{20}(Z,\tau)],$$

$$\rho_2=\frac{N^2}{gk}[r_2(Z,\tau)\exp 2iX+r_{20}(Z,\tau)] \tag{21}$$

and $U_2=\partial\phi_{20}/\partial Z$ is the Eulerian-mean second-order flow and $F(\tau)$ is a yet unspecified function of τ. Real parts of ψ_2,ρ_2 are to be taken and * represents complex conjugates.

The boundary conditions are

$$\phi_2 = 0 \quad \text{at} \quad Z = kh,$$

and

$$\phi_2 = -\frac{A^2\tau}{4}\sin\alpha - \frac{A}{2}\frac{\partial\phi}{\partial Z} \quad \text{at} \quad Z = -kh.$$

These equations can be solved using the same numerical procedure as before calling, at each time step, on the first order solution when calculating the terms which appear on the right hand side of the equations. In modelling the experiments in which the tube is returned to a horizontal position (at time t_0 say) the terms including $\tau\sin\alpha$ became constant with τ equal to Nt_0, and elsewhere α is made equal to zero.

We now consider the appropriate way to specify $F(\tau)$ and to find the function of Z which arises when (20) is integrated.

3.2. *Mean flow and density fields*

In the laboratory experiments the volume flux across any vertical plane normal to the tube axis must, by continuity, be zero since the tube is closed at the ends. A non-zero flux would imply that the volume between the plane and an end wall was changing. The average volume flux is

$$\int_{-h+\eta}^{h}\left(U+\frac{\partial\psi}{\partial z}\right)dz = 0. \tag{22}$$

Performing the integration and using the boundary conditions (11), (12), we find, correct to order ϵ^2,

$$\int_{-kh}^{kh} U_2\,dZ = \frac{\tau}{4}A^2\sin\alpha + \frac{A}{2}\frac{\partial\phi}{\partial Z}(-kh). \tag{23}$$

But using equation (18)

$$\int_{-kh}^{kh}\frac{\partial U_2}{\partial\tau}dZ = \frac{i}{2}khA\tau\sin\alpha\frac{\partial\phi}{\partial Z} + 2khF(\tau),$$

and hence

$$F(\tau) = \frac{1}{8kh}\left\{A^2\sin\alpha + 2A\left(\frac{\partial}{\partial\tau} + iZ\tau\sin\alpha\right)\frac{\partial\phi}{\partial Z}\right\} \tag{24}$$

evaluated at $Z = -kh$. In the laboratory experiments, the flow is initially at rest and so (18), with (24), is to be solved with $U_2 = 0$ at $\tau = 0$.

We can find the relevant solution of (20) by the following argument. Consider now the wave displacement, $\zeta(x, z_0, t)$, at level z_0. This is found by specifying that the surface $z_0 + \zeta$ shall be one of constant density (Thorpe 1978*b*). Using the expression for the density below (9) we find

$$\zeta = \frac{g}{N^2}\rho(x, z_0+\zeta, t). \tag{25}$$

If $\zeta = \epsilon\zeta_1 + \epsilon^2\zeta_2 + \ldots$ this gives

$$\zeta_1 = \frac{g}{N^2}\rho_1(x, z_0, t) \tag{26}$$

and

$$\zeta_2 = \frac{g}{N^2}\left(\zeta_1\frac{\partial\rho_1}{\partial z} + \rho_2\right). \tag{27}$$

For an infinite tube, or a finite one before the surges arrive from the ends, we expect the volume of fluid lying below a given density surface in the middle section of the tube to be conserved. Then $\bar{\zeta} = 0$ and (13), (26) and (27) imply that

$$r_{20} = -\frac{1}{4}\frac{\partial}{\partial Z}|r^2|. \tag{28}$$

Differentiating (28) with respect to τ and using (15), we see that (28) satisfies (20), and the initial condition of no disturbance (implying $\rho_1 = \rho_2 = 0$ initially). This checks the correctness of (28).

The equations (26), (27) serve to define the surfaces of constant density, the dye lines in the laboratory experiments.

3.3. *Mean drift*

Internal waves generate a second-order Stokes drift which has been estimated and observed in laboratory experiments (Thorpe 1968*b*). Here we estimate the drift associated with waves caused by the accelerating flow over the sinusoidal floor. Relative to the frame of reference fixed in the floor, the co-ordinates of a particle in the flow described in (3.1) may be written

$$\begin{aligned} x &= \tfrac{1}{2}N^2 z_0 t \sin\alpha + x_0 + \epsilon x_1 + \epsilon^2 x_2 + \dots \\ z &= z_0 + \epsilon z_1 + \epsilon^2 z_2 + \dots, \end{aligned} \tag{30}$$

(see Thorpe 1978*b*) where $x_1, x_2, z_1, z_2, \dots$ are functions of x_0, z_0 and t. The speed of the particle is given by

$$\frac{dx}{dt} = N^2 tz \sin\alpha + \epsilon\psi_{1,z} + \epsilon^2\psi_{2,z} + \dots, \tag{31}$$

$$\frac{dz}{dt} = -\epsilon\psi_{1,x} - \epsilon^2\psi_{2,x} - \dots, \tag{32}$$

evaluated at x, z. Transferring to non-dimensional co-ordinates $X_0 = kx_0, Z_0 = kz_0$, these equations give, to order ϵ:

$$\left(\frac{\partial}{\partial\tau} + iZ_0\tau\sin\alpha\right) X_1 = Z_1\tau\sin\alpha + \frac{\partial\phi}{\partial Z_0}, \tag{33}$$

$$\left(\frac{\partial}{\partial\tau} + iZ_0\tau\sin\alpha\right) Z_1 = -i\phi, \tag{34}$$

where

$$kx_1 = X_1(Z_0, \tau)\exp i\xi,$$

$$kz_1 = Z_1(Z_0, \tau)\exp i\xi,$$

and

$$\xi = X_0 + \tfrac{1}{2}Z_0\tau^2\sin\alpha,$$

whilst to order ϵ^2:

$$\left(\frac{\partial}{\partial\tau} + 2iZ_0\tau\sin\alpha\right) X_2 = Z_2\tau\sin\alpha + \frac{\partial\phi_2}{\partial Z_0} + \frac{1}{2}\left(Z_1\frac{\partial^2\phi}{\partial Z_0^2} + iX_1\frac{\partial\phi}{\partial Z_0}\right), \tag{35}$$

$$X_{20,\tau} = Z_{20}\tau\sin\alpha + U_2(Z_0, \tau) + \frac{1}{2}\left(Z_1\frac{\partial^2\phi^*}{\partial Z_0^2} - iX_1\frac{\partial\phi^*}{\partial Z_0}\right), \tag{36}$$

$$\left(\frac{\partial}{\partial\tau}+2iZ_0\tau\sin\alpha\right)Z_2=-2i\phi_2+\frac{1}{2}\left(X_1\phi-iZ_1\frac{\partial\phi}{\partial Z_0}\right), \tag{37}$$

$$Z_{20}=\tfrac{1}{2}i[X_1^*Z_1-X_1^*(Z_0,0)\,Z_1(Z_0,0)], \tag{38}$$

where

$$kx_2=X_2(Z_0,\tau)\exp 2i\xi+X_{20}(Z_0,\tau),$$

$$kz_2=Z_2(Z_0,\tau)\exp 2i\xi+Z_{20}(Z_0,\tau),$$

and real parts are to be taken. The initial displacements are zero.

Equation (36) now gives the wave contribution to the Lagrangian drift speed. It contains the Eulerian drift contribution U_2 and supplementary terms corresponding to the Stokes drift.

3.4. *Comparison with experiments*

The wave displacements (26), (27), have been calculated for the conditions and scales appropriate to the experiments and, for comparison, are shown in figures 3 and 4, correct to orders ϵ and ϵ^2. The early development of the waves, and their later phase and amplitude are well described by linear (order ϵ) theory. The waves appear to propagate vertically more rapidly than predicted by figure 2. In the JWKB approximation equation (6) shows that the vertical wave number, m, of the waves becomes small and then imaginary as τ increases, so that the lines of constant phase will tend to become vertical near the lower boundary, as indeed observed. The vertical group velocity c_{gv}, also becomes imaginary, (7) implying that waves cannot continue to be radiated vertically away from the boundary. There is some evidence in the photographs that in the vicinity of the boundary the wave amplitude decreases, which is also consistent with m becoming imaginary giving an exponential decrease in wave amplitude with height.

When the mean flow Richardson number falls below about 1·5 the waves become distorted from the sinusoidal, linear solution, profile. The second-order (ϵ^2) terms account for much of this distortion until the mean flow Richardson number falls below about 0·5 in the accelerating flow or until gravitational overturn becomes imminent. We have used the numerically calculated stream function and density to estimate the local Richardson in the flow (as in Geller *et al.* 1975). The regions in which this is less than 0·25 or zero are shown in figures 3 and 4. The regions lie in places where the dye lines are thickened; regions of high density gradient have relatively large Richardson numbers. The onset and position of gravitational overturn are surprisingly well predicted by the model. This suggests that the development of high harmonics in the final stages of overturn occurs very rapidly and locally in those parts of the flow in which the density gradient has already been significantly reduced by the first and second-order effects. The low Richardson number regions are tilted, about 1 cm thick, and negative values of Richardson number are found near the upper edge of the regions in which the Richardson number is less than 0·25, a feature found by Fritts (1978) in his numerical computations. In the last stages of development followed in the laboratory experiments gravitational overturn can be seen simultaneously at several levels well below the mid-depth of the tube and this pattern is reflected in the numerical computations.†

† It seems likely, referring to figure 2, that this effect may be due to internal waves generated during acceleration, which find their critical levels well below the level $z = 0$. Caution is needed, however, in interpreting figure 2 because of the invalid JWKB approximation.

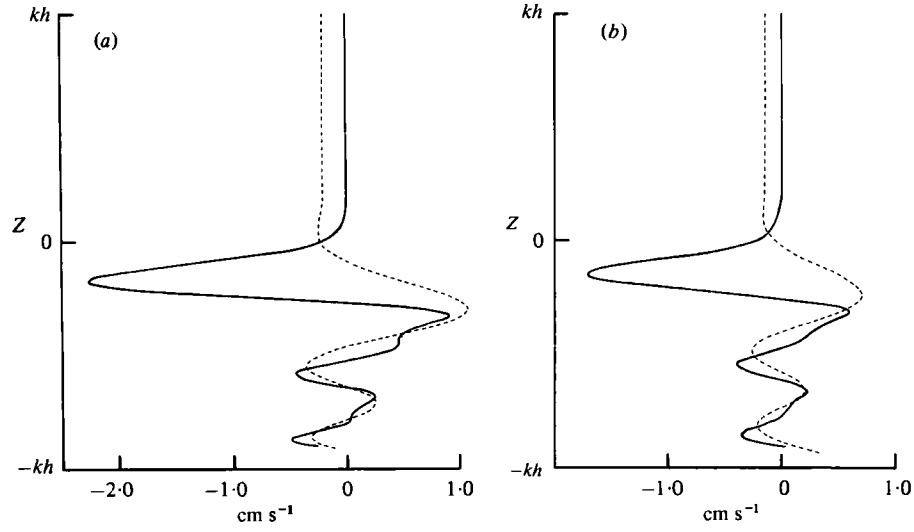

FIGURE 7. Mean second order Stokes drift (solid line) and Eulerian mean second-order flow (dashed) corresponding to conditions of (*a*) figure 3 at $Nt = 14{\cdot}52$, (*b*) figure 4 at $Nt = 14{\cdot}00$.

The calculated mean second-order Eulerian flow is shown in figures 3 and 4. In the later stages of development of the waves it is dominated by a 'jet' just below the critical layer directed against the mean flow at that level. The occurrence of such jets and their effects on the critical layer have been discussed by Breeding (1971) and Fritts (1978). The estimated strength of the jets is quite small and it was not possible in the experiments to measure the x-averaged velocity with sufficient accuracy to resolve the jet in the presence of the large mean shear flow and waves. The large flows near the lower boundary which appear in the numerical calculations result from the initial conditions there (see § 3.2).

The Stokes second-order drift has also been calculated (from 36), and this is shown in figure 7, together with the mean second-order Eulerian flow. The sum of the Eulerian-mean flow and Stokes drift gives the Lagrangian-mean flow, and this differs considerably from the Eulerian-mean flow, the jet being significantly modified and the upper part reversed by the Stokes drift. The maximum Stokes drift is in the same direction as the flow U below the critical layer. This is a feature reminiscent of the sense of maximum drift in gravity waves of first mode in a hyperbolic tangent density profile and zero mean flow, or of the drift near the maximum displacement of first mode waves in a constant density gradient and zero mean flow (Thorpe 1968*b*) when the drift is opposed in direction to the phase speed of the waves. Here the local phase speed relative to the mean flow is to the right, whilst the relative maximum drift is to the left, and again the two are opposite in direction. The Stokes drift is anomalous close to the floor of the tube since particles which originate near the bottom of the troughs of the corrugations ($z_0 = -h - |\eta|$ at $t = 0$) and approximately follow their shape will, in the mean, have a net upwards displacement ($Z_{20} \neq 0$). They are transferred, on average, into a region where the mean flow is less and will, on this account, have a smaller total drift than that appropriate to their level of origin.

4. Discussion

4.1. *Viscous effects*

The experiments and numerical model show that the critical layer inhibits the vertical propagation of waves even at low Richardson numbers and that gravitational instability is found even when the mean-flow Richardson number is about one. No Kelvin–Helmholtz instability was observed in the experiments. This may have been due to the particular density and velocity profile chosen (which, as we remarked in the introduction, is probably stable even at small Richardson numbers), or to the slow growth of the instabilities in the wave-distorted velocity and density fields, or to viscosity, ignored in the computations. Hazel (1967) examined the effect of viscosity on the basic critical-layer problem and found it to be important to a distance about

$$5[\nu/(k\,\partial U/\partial z)]^{\frac{1}{3}}$$

below the critical layer, where ν is the kinematic viscosity. This thickness is 1·10 cm when the mean flow Richardson number was 0·5 for the conditions of figure 3, whilst for those of figure 4 it is 1·23 cm. Although Hazel's theory is for steady flow and the depth range of viscous influence does not overlap fully with the tilted regions in which the local Richardson number is small, the fact that the length scales are similar suggests that, as in the earlier experiments, viscosity may inhibit Kelvin–Helmholtz instability near the critical layer (Fritts & Geller 1976). Even in the experiment of figure 5 with increased wavelength, where the region in which the Richardson number was less than 0·25 was calculated to be 2·0 cm in depth and the viscous layer 1·4 cm thick at a mean flow Richardson of 0·5, it is possible that Kelvin–Helmholtz instability was suppressed by viscous effects.† The general agreement between the experiments and numerical computations suggests, however, that viscosity does not significantly affect the displacement field.

4.2. *Related experiments*

Some experiments were made with density and velocity profiles containing narrow gradient regions between uniform layers. These flows are known to be unstable when the mean flow Richardson number is less than one quarter, and it was hoped that Kelvin–Helmholtz instability might be excited near the critical layer by waves when the mean flow itself was stable to infinitesimal disturbances. An asymmetrical profile (thin lower layer) of density was chosen so that if Kelvin–Helmholtz instability occurred it would not only have an expected scale different from the boundary undulations, but would be a propagating disturbance (e.g. see Thorpe 1973*b*, figure 13 and text). Figure 8 shows a flow with a density gradient, marked by three layers of dye, between two homogeneous layers. The tube was tilted for only 3·30 s after which the minimum 'undisturbed' mean flow Richardson number was 0·627, and the mean flow was thus stable. Waves developed and 'broke' near the critical layer in the density gradient region. (It is interesting to compare this with the breaking of pre-existing internal waves in an accelerating shear flow shown in figure 7, Thorpe 1978*a*.) Small-scale waves which may be due to Kelvin–Helmholtz instability can be seen in

† Professor O. M. Phillips has shown me a film of his experiments in a continuously stratified water tunnel in which billows resulting from Kelvin–Helmholtz instability can be seen in the vicinity of the critical layer.

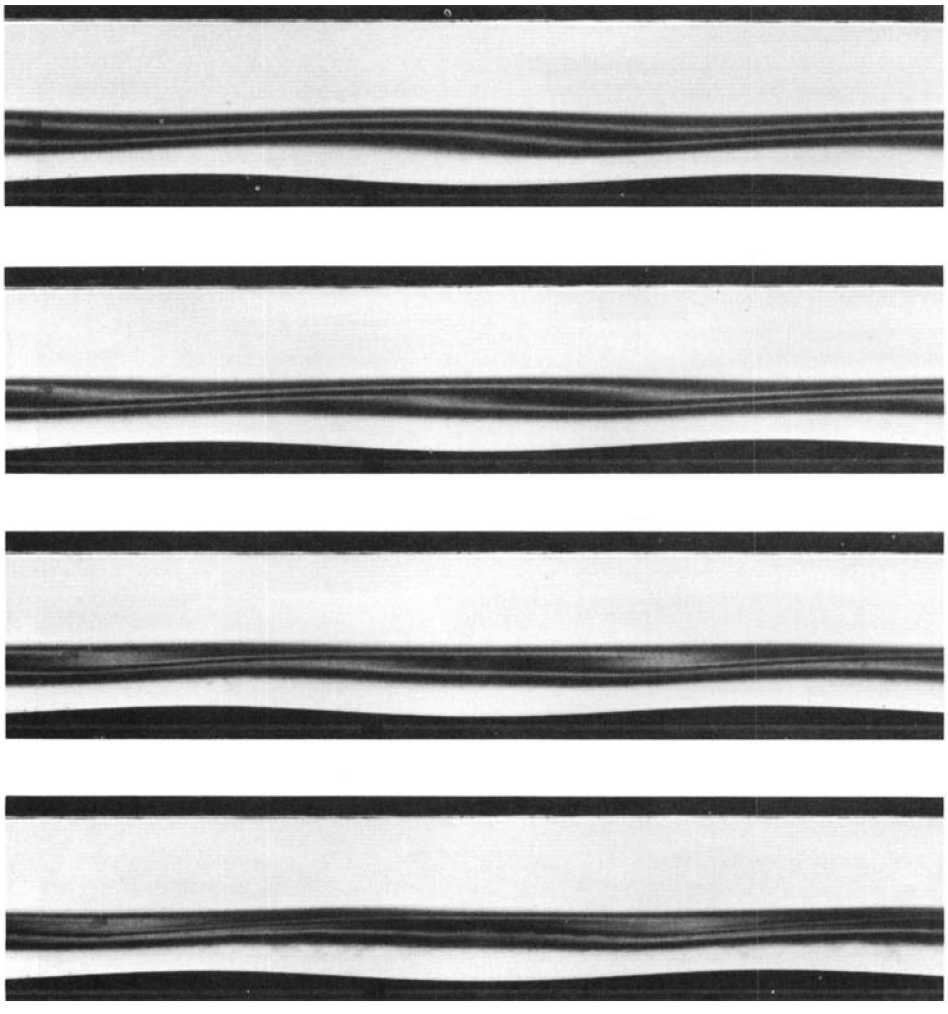

FIGURE 8. Waves in a three-layer fluid over 0·5 cm amplitude corrugations of length 50 cm. Upper and lower fluids are of uniform density and the density gradient in the middle layer is almost uniform with $N = 4{\cdot}19$ rad s^{-1}. The tube was tilted through 5·2 deg from 3·30 s giving a minimum mean flow Richardson number of 0·63. Photographs are at time (*a*) 4·77 s, (*b*) 7·23 s, (*c*) 9·70 s and (*d*) 12·18 s.

the lower due line in figure 8(*d*), but occur only after the gravitational overturn near the critical layer.

An example with two density interfaces is shown in figure 9. In this experiment the density profile was measured by a single-electrode conductivity probe before the tube was tilted, and the Richardson numbers quoted in the figure caption were calculated from the estimated mean flow (Thorpe 1968*a*). The experiment shows the development of a variety of scales at low Richardson number in an accelerating flow. The critical layer was in the upper interface, flow below this level being to the left. Waves grew first at the lower interface, their crests being slightly to the right of the corrugation crests (*a*), but then the two became approximately in phase and a small region

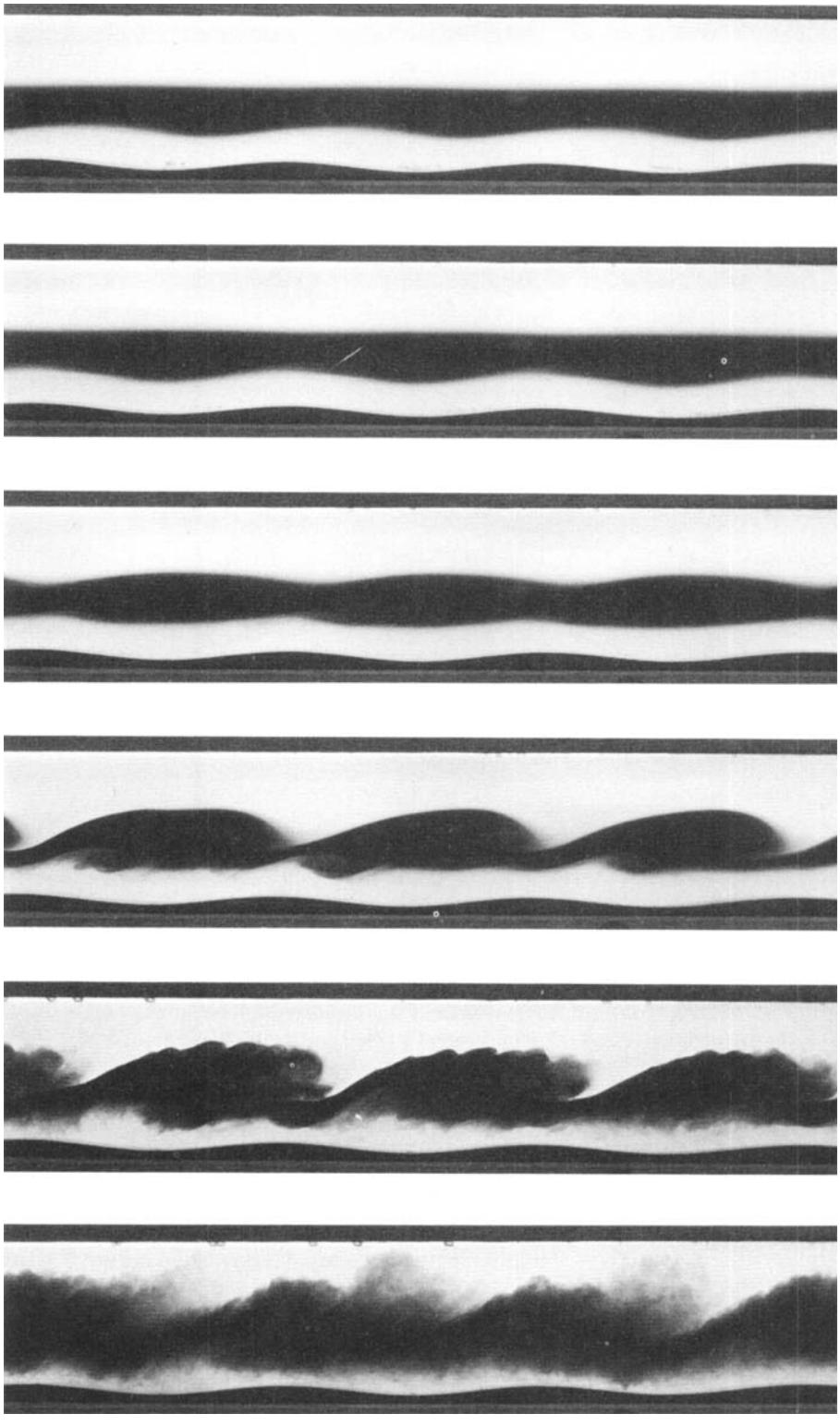
(a)
(b)
(c)
(d)
(e)
(f)

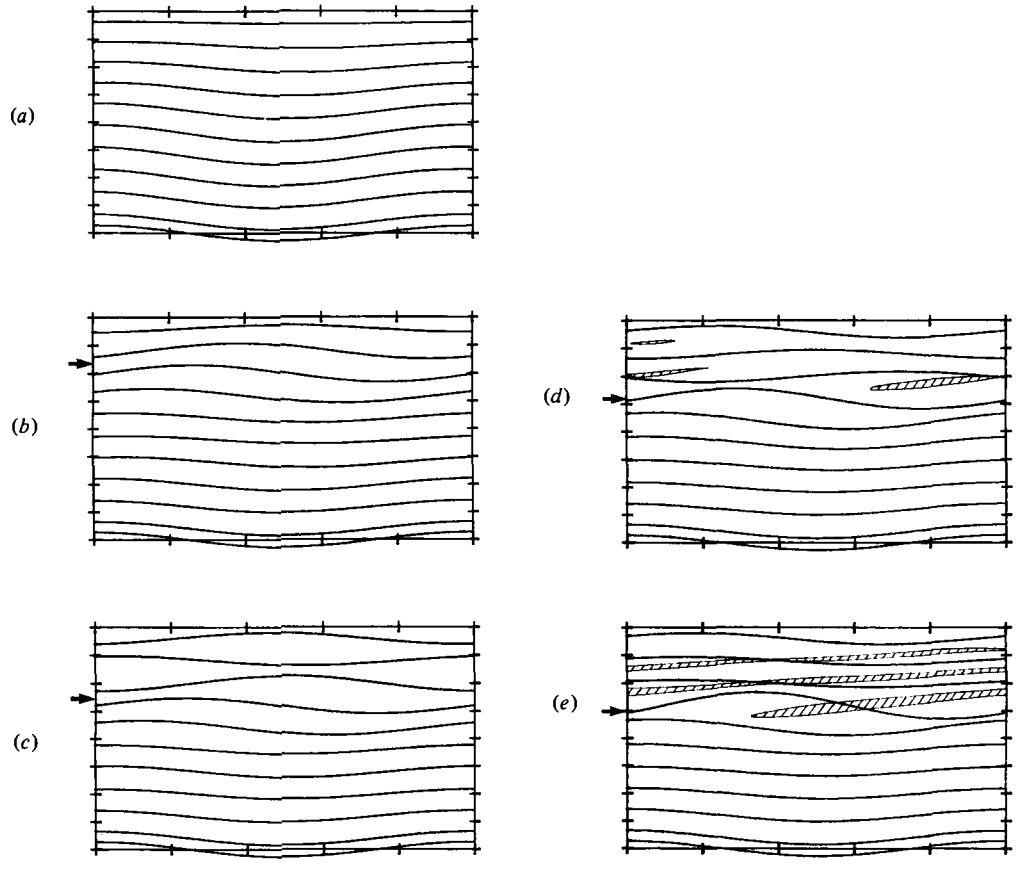

FIGURE 10. Numerical model of flow with $V = -0{\cdot}864$, $kh = 1{\cdot}85$, $A = 0{\cdot}126$, $\alpha = 0{\cdot}09$ rads at times Nt: (*a*) 2·94, (*b*) 8·74, (*c*) 14·55, (*d*) 17·45, (*e*) 20·35, showing linear (order ϵ) solutions and hatched regions of negative density gradient. The level of the critical layer is shown by the arrows.

of overturning appeared at the wave crests (*b*). This region advected to the right, through the waves, being amplified when it reached the succeeding wave crest (*c*). Soon thereafter secondary waves, about one third of the length of the corrugations (and seven or eight times the interface thickness) grew between the sites of the initial instability (*d*), developing in the familiar pattern of Kelvin–Helmholtz 'billows'. Waves at the upper interface appeared soon after the first signs of overturn at the lower interface, and were 180 deg out of phase with the corrugations on the floor. These waves became larger than the waves on the lower interface and overturning occurred at their troughs (*c*). The crests were much flatter than the troughs (*d*), and on the crests small billows developed (*e*) which grew as they moved to the right. Flow eventually became highly disordered (*f*).

FIGURE 9. Waves in a three-layer fluid over 0·5 cm amplitude corrugations of length 25 cm. The layers are uniform and the density difference between neighbouring fluids is equal to 0·0444 g cm^{-3}. The upper layer is twice the thickness of the two lower layers, which are of equal depth, and some diffusion has occurred between layers. Photographs are at the following times (the mean-flow Richardson numbers are given in brackets for the upper and lower interfaces respectively): (*a*) 3·08 s (0·231, 0·272), (*b*) 4·64 s (0·102, 0·120), (*c*) 6·19 s (0·057, 0·067), (*d*) 7·36 s (0·040, 0·048), (*e*) 8·53 s (0·030, 0·035) and (*f*) 9·70 s (0·023, 0·027).

4.3. *Oceanographic applications*

The importance of critical-layer effects on the spectrum of internal gravity waves in the ocean has yet to be established (Munk 1980). It is likely, however, that inertial waves modify the internal wave spectrum by producing critical layers. There is evidence that near-inertial waves are generated near the sea surface by wind (Pollard & Millard 1970), and spread downwards through the water column (their phase speed is however upwards) producing transient regions of local shear across which the velocity difference is large. These are illustrated very clearly in Sandford's (1975) and Rossby & Sandford's (1976) vertical profiles of current. When the front of an inertial wave group arrives, pre-existing free internal gravity waves with sufficiently large horizontal phase speed will interact with the flow generated by the inertial waves, be modified by the shear, and may break if their particle speeds exceed the modified phase speed (Thorpe 1978*a*, *b*) but will not encounter critical layers. Those waves with small phase speeds, for example those which are topographically generated or which, through the nature of their forcing, are locked to low horizontal speeds, will encounter critical layers produced by the relatively larger horizontal currents of the inertial waves and be subjected to the effects discussed above.

It is beyond the scope of this paper to discuss these, or other wave–wave critical-layer interactions in detail, but to illustrate their nature a numerical experiment was made to examine the effect of a transient, vertically propagating critical layer. An initial wave was set up by passing z-independent flow, U_0, over the sinusoidal floor of the tube. A uniformly accelerating shear flow was then superimposed so as to give a basic flow $U = U_0 + N^2tz\sin\alpha$. The appropriately modified linearized equations are given in the appendix. For $U_0 < 0$ the mean flow over the corrugated floor is initially entirely in the negative x-direction, but when $t > -U_0/(N^2h\sin\alpha)$ there is a region near the top of the tube in which the flow is positive. A critical layer exists at height $z = -U_0/(N^2t\sin\alpha)$, descending towards $z = 0$ as t increases. Large waves are found in the neighbourhood of the critical layer (figure 10) with a variable field of relatively high vertical wave-number waves above the layer. The transcience of the layer does not inhibit wave amplification in its vicinity.

The effects of transient or vertically propagating critical layers and their geophysical significance deserve further study.

It is a pleasure to acknowledge the assistance of Mr M. Bray in making the laboratory experiments. I am indebted to Dr M. E. McIntyre and Mr D. Broutmann for bringing to my attention errors in the first draft.

Appendix

Consider the effect of moving the corrugated flow of the laboratory tube to the left at uniform speed U, providing a steady wave pattern, before the tube is fitted. This is equivalent to having initially a uniform flow over a stationary boundary. Subsequently the flow distorts. Choosing axes moving with the floor $U = U_0 + N^2tz\sin\alpha$, and equation (14), (15) become

$$\left[\frac{\partial}{\partial\tau} + i(V + Z\tau\sin\alpha)\right]\theta + \left(\sin\alpha\frac{\partial}{\partial Z} - i\cos\alpha\right)r = 0 \qquad \text{(A 1)}$$

and

$$\left[\frac{\partial}{\partial\tau}+i(V+Z\tau\sin\alpha)\right]r+i\phi=0, \tag{A 2}$$

where $V=U_0k/N$, with boundary conditions

$$\phi=0 \quad \text{at} \quad Z=kh,$$
$$\phi=-A(V+Z\tau\sin\alpha) \quad \text{at} \quad Z=-kh.$$

The appropriate initial conditions can be found by putting $\partial/\partial\tau=0$ and $\alpha=0$ in (A 1) and (A 2). Solving these we find

$$\phi=-AVf(V,Z), \quad r=-\phi/V,$$

where

$$f(q,Z)=\frac{H[\gamma(q)(kh-Z)]}{H[2\gamma(q)kh]}$$

with

$$H[y]=\begin{cases}\sin y, & \gamma=(1-q^2)^{\frac{1}{2}}/V, \quad \text{if} \quad q<1,\\ y, & \gamma=1, \quad \text{if} \quad q=1,\\ \sinh y, & \gamma=(q^2-1)^{\frac{1}{2}}/V, \quad \text{if} \quad q>1.\end{cases}$$

We assume that the denominator of the expression for f is non-zero so that resonant waves are excluded.

REFERENCES

Acheson, D. J. 1976 On over-reflexion. *J. Fluid Mech.* **77**, 433–472.

Booker, J. R. & Bretherton, F. P. 1967 The critical layer for internal gravity waves in a shear flow. *J. Fluid Mech.* **27**, 513–539.

Breeding, R. J. 1971 A non-linear investigation of critical levels for internal atmospheric gravity waves. *J. Fluid Mech.* **50**, 545–563.

Bretherton, F. 1966 The propagation of groups of internal gravity waves in shear flow. *Quart. J. Roy Met. Soc.* **92**, 466–480.

Brown, S. N. & Stewartson, K. 1980*a* On the nonlinear reflexion of a gravity wave at a critical level. *J. Fluid Mech.* **100**, 577–595.

Brown, S. N. & Stewartson, K. 1980*b* On the algebraic decay of disturbances in a stratified linear shear flow. *J. Fluid Mech.* **100**, 811–816.

Eymard, L. & Weill, A. 1979 A study of gravity waves in the planetary boundary layer by acoustic sounding. *Boundary-layer Met.* **17**, 231–246.

Fritts, D. C. 1978 The non-linear gravity wave-critical level interaction. *J. Atmos. Sci.* **35**, 397–413.

Fritts, D. C. 1979 The excitation of radiating waves and Kelvin–Helmholtz instabilities by the gravity wave-critical level interaction. *J. Atmos. Sci.* **36**, 12–23.

Fritts, D. C. & Geller, M. A. 1976 Viscous stabilization of gravity wave critical layer flows. *J. Atmos. Sci.* **33**, 2276–2284.

Garrett, C. J. R. 1968 On the interaction between internal gravity waves and a shear flow. *J. Fluid Mech.* **34**, 711–720.

Geller, M. A., Tanaka, H. & Fritts, D. C. 1975 Production of turbulence in the vicinity of critical levels for internal gravity waves. *J. Atmos. Sci.* **32**, 2125–2135.

Grimshaw, R. 1980 A general theory of critical level absorption and valve effects for linear wave propagation. *Geophys. Astrophys. Fluid Dynamics* **14**, 303–326.

Hazel, P. 1967 The effects of viscosity and heat conduction on internal gravity waves at a critical level. *J. Fluid Mech.* **30**, 775–784.

KLOSTERMEYER, J. 1980 Computation of acoustic-gravity waves, Kelvin–Helmholtz instabilities and wave-induced eddy transport in realistic atmospheric models. *J. Geophys. Res.* **85**, 2829–2840.

MCINTYRE, M. E. & WEISSMAN, M. A. 1978 On radiating instabilities and resonant overreflexion. *J. Atmos. Sci.* **35**, 1190–1196.

MERRILL, J. T. 1977 Observational and theoretical study of shear instability in the airflow near the ground. *J. Atmos. Sci.* **34**, 911–921.

MUNK, W. H. 1980 Internal waves and small scale processes. In *Evolution of Physical Oceanography* (ed. B. A. Warren & C. Wunsch), pp. 264–291. Massachusetts Institute of Technology Press.

PEREGRINE, D. H. & THOMAS, G. P. 1979 Finite amplitude deep-water waves on currents. *Phil. Trans. Roy. Soc.* A **292**, 371–390.

POLLARD, R. T. & MILLARD, R. C. 1970 Comparison between observed and simulated wind-generated inertial oscillations. *Deep Sea Res.* **17**, 813–821.

ROSSBY, H. T. & SANDFORD, T. B. 1976 A study of velocity profiles through the main thermocline. *J. Phys. Oceanog.* **6**, 766–774.

SANDFORD, T. B. 1975 Observations of the vertical structure of internal waves. *J. Geophys. Res.* **80**, 3861–3871.

STEWARTSON, K. 1978 The evolution of the critical layer of a Rossby wave. *Geophys. Astrophys. Fluid Dyn.* **9**, 185–200.

TANEKA, H. 1975 Turbulent layers associated with a critical level in the planetary boundary layer. *J. Met. Soc. Japan* **53**, 425–439.

THORPE, S. A. 1968*a* A method of producing a shear flow in a stratified fluid. *J. Fluid Mech.* **32**, 693–704.

THORPE, S. A. 1968*b* On the shape of progressive internal waves. *Phil. Trans. Roy. Soc.* A **263**, 563–614.

THORPE, S. A. 1971 Experiments on the instability of stratified shear flows: miscible fluids. *J. Fluid Mech.* **46**, 299–319.

THORPE, S. A. 1973*a* Turbulence in stably stratified fluids. A review of laboratory experiments. *Boundary-layer Met.* **5**, 95–119.

THORPE, S. A. 1973*b* Experiments on instability and turbulence in a stratified shear flow. *J. Fluid Mech.* **61**, 731–751.

THORPE, S. A. 1978*a* On internal gravity waves in an accelerating shear flow. *J. Fluid Mech.*, 623–639.

THORPE, S. A. 1978*b* On the shape and breaking of finite amplitude internal gravity waves in a shear flow. *J. Fluid Mech.* **85**, 7–31.